Mathematical framework of the PITM method for the simulation of turbulent flows

Bruno Chaouat[1], Roland Schiestel[2]

[1] *ONERA, Université Paris-Saclay, 92322 Châtillon, France*
[2] *IRPHE, 13384, Marseille, France.*

Abstract

We present the mathematical framework of the PITM method in the spectral space of wave numbers from a physical standpoint. This framework is then used to develop subfilter turbulence models accounting for the main physical process such as production, dissipation and transfer of turbulence energy. Then, we present briefly several flows encountered in engineering applications to show that the PITM method gains interest not only from a theoretical point of view but also from a practical point of view for users involved in CFD.

1 Background and rationale

Different methods have been developed in the past fifty years for simulating turbulent flows [1, 2]. On the one hand, the direct numerical simulation (DNS) is obviously the best tool to consider but it is out of reach up to present day for practical complex applications, even if using supercomputers. Large eddy simulation (LES) is a promising method but still remains also extremely costly in computer resources at large Reynolds numbers [3]. On the other hand, the Reynolds Averaged Navier-Stokes (RANS) method works relatively well for quasi-steady flows in the mean [4] but shows however some weaknesses in capturing the large scale turbulent eddies [5]. To overcome these difficulties, researchers have developed hybrid RANS/LES methods in the past two-decade to simulate industrial flows on coarse grids with acceptable computer resources. These main schools of hybrid RANS/LES modelling [6] are the very large eddy simulation (VLES) [7], detached eddy simulation (DES) [8], partially integrated transport modelling (PITM) [9, 10, 11], partially averaged Navier-Stokes (PANS) [12] and scale adaptive approach (SAS) [13]. Contrarily to zonal hybrid models often based on empirical techniques with the overwhelming problems caused by the so-called gray zone, the PITM method [9, 10, 11], gains a major interest both from a theoretical and practical point of view because it bridges the RANS and LES methodologies with seamless coupling and allows to perform numerical simulations of turbulent flows out of spectral equilibrium on relatively coarse grids. In this present work, we will focus on the mathematical framework of the PITM method developed in the spectral space [14] and we will briefly present some cases of application to complex flows [15].

2 The PITM method

2.1 Filtering process

In RANS methodology, each variable ϕ can be decomposed into a statistical part $\langle\phi\rangle$ and a fluctuating part ϕ' such that $\phi = \langle\phi\rangle + \phi'$ whereas in large eddy simulation, the variable ϕ is decomposed into a large scale (or resolved part) $\bar{\phi}$ and a subfilter-scale fluctuating part $\phi^>$ or modeled part such that $\phi = \bar{\phi} + \phi^>$. The instantaneous fluctuation ϕ' contains the large scale fluctuating part $\phi^<$ and the small scale fluctuating part $\phi^>$ such that $\phi' = \phi^< + \phi^>$. The filtered variable $\bar{\phi}$ is defined by the filtering operation as the convolution with a filter G in space $\overline{\phi} = G * \phi$ that leads to the computation of a variable convolution integral

$$\bar{\phi}(\boldsymbol{x}, t) = \int_\Omega G\left[\boldsymbol{x} - \boldsymbol{\xi}, \Delta(\boldsymbol{x}, t)\right] \phi(\boldsymbol{\xi}, t) d\boldsymbol{\xi} \qquad (1)$$

where in this expression, Δ denotes the filter-width that varies in time and space and Ω denotes the flow domain. Obviously, the properties of the filtering operator are different from those of the statistical averaging process so that there is no direct connection between the averaged field in a statistical sense and the filtered field in LES. All these difficulties may disappear if considering the tangent homogeneous anisotropic turbulence field at the physical space location $\boldsymbol{X}$ within the nonhomogeneous field [14]. In this framework, the variation of the mean velocities u_k is accounted for by the use of Taylor series expansion in space limited to the linear terms such that $\langle u_k\rangle (X_m + \xi_m) = \langle u_k\rangle (X_m) + \Lambda_{kj}\xi_j$ where Λ_{kj} is a constant tensor and we recover the interesting property establishing the link between the RANS and LES methodologies [14, 17]

$$\overline{\langle u_k\rangle}(X_m + \xi_m) = \langle u_k\rangle (X_m) \qquad (2)$$

Strictly speaking, $\overline{\langle\phi\rangle} = \langle\bar{\phi}\rangle = \langle\phi\rangle$ stands only in the tangent homogeneous space. In practice however, one can assume that $\langle\bar{\phi}\rangle \approx \langle\phi\rangle$ if the variation of the flow velocities over the filter width is not too large.

2.2 Basic equations in the spectral space

2.2.1 Turbulent velocity fields

The PITM method finds its physical foundation in the spectral space of wave vectors [14]. The theory deals with the dynamic equation of the two-point fluctuating velocity correlations in their extensions to nonhomogeneous turbulence. By using the Fourier transform given by

$$\widehat{\phi}(\boldsymbol{X}, \boldsymbol{\kappa}) = \int \phi(\boldsymbol{X}, \boldsymbol{\xi}) \exp\left(-j\boldsymbol{\kappa}\boldsymbol{\xi}\right) d\boldsymbol{\xi} \qquad (3)$$

and performing averaging on spherical shells on the dynamic equation defined as [16]

$$[\phi(\boldsymbol{X})]^\Delta(\kappa) = \frac{1}{A(\kappa)} \oiint_{A(\kappa)} \widehat{\phi}(\boldsymbol{X}, \boldsymbol{\kappa})\, dA(\kappa) \qquad (4)$$

where $A(\kappa)$ denotes the spherical shell of radius κ, it is then possible to derive the evolution equation of the spectral velocity correlation tensor in one-dimensional spectral space accounting for the spectral terms of transfer, production and dissipation that play a crucial role in PITM. As a result, the transport equation of the spherical average of the Fourier transform of the two-point correlation tensor $\varphi_{ij}(\boldsymbol{X},\kappa) = \left\langle u_i' u_j'(\boldsymbol{X})\right\rangle^{\Delta}(\kappa)$ reads [14]

$$\frac{\partial \varphi_{ij}(\boldsymbol{X},\kappa)}{\partial t} + \langle u_k\rangle(\boldsymbol{X})\frac{\partial \varphi_{ij}(\boldsymbol{X},\kappa)}{\partial X_k} = \mathcal{P}_{ij}(\boldsymbol{X},\kappa) + \mathcal{T}_{ij}(\boldsymbol{X},\kappa) + \Psi_{ij}(\boldsymbol{X},\kappa) + \mathcal{J}_{ij}(\boldsymbol{X},\kappa) - \mathcal{E}_{ij}(\boldsymbol{X},\kappa) \quad (5)$$

where in this equation, the function φ_{ij} denotes the spherical mean of the Fourier transform of the two-point velocity correlation tensor, $\mathcal{P}_{ij}$ represents the production term, $\mathcal{T}_{ij}$ is the total transfer term, Ψ_{ij} is the redistribution term, $\mathcal{J}_{ij}$ embodies all the diffusion like terms, and $\mathcal{E}_{ij}$ denotes the stress dissipation rate, $\boldsymbol{X}$ is located midway between the two points and κ is the wave number. In particular, the production term $\mathcal{P}_{ij}$ is given by

$$\mathcal{P}_{ij}(\boldsymbol{X},\kappa) = -\varphi_{ik}(\boldsymbol{X},\kappa)\frac{\partial \langle u_j\rangle}{\partial X_k} - \varphi_{jk}(\boldsymbol{X},\kappa)\frac{\partial \langle u_i\rangle}{\partial X_k} \quad (6)$$

and the dissipation term $\mathcal{E}_{ij}$ is defined by

$$\mathcal{E}_{ij}(\boldsymbol{X},\kappa) = \frac{\nu}{2}\frac{\partial^2 \varphi_{ij}(\boldsymbol{X},\kappa)}{\partial X_l X_l} + 2\nu\kappa^2\varphi_{ij}(\boldsymbol{X},\kappa) \quad (7)$$

where ν stands for the molecular viscosity. The equation for the turbulence energy spectrum $E = \varphi_{jj}/2$ is simply obtained by tensorial contraction of (Eq. (5)) leading to

$$\frac{\partial E(\boldsymbol{X},\kappa)}{\partial t} + \langle u_i\rangle(\boldsymbol{X})\frac{\partial E_{ij}(\boldsymbol{X},\kappa)}{\partial X_j} = \mathcal{P}(\boldsymbol{X},\kappa) + \mathcal{T}(\boldsymbol{X},\kappa) + \mathcal{J}(\boldsymbol{X},\kappa) - \mathcal{E}(\boldsymbol{X},\kappa) \quad (8)$$

where $\mathcal{P} = \mathcal{P}_{mm}/2$, $\mathcal{T} = \mathcal{T}_{mm}/2$, $\mathcal{J} = \mathcal{J}_{mm}/2$ and finally, $\mathcal{E} = \mathcal{E}_{mm}/2$. In the following, we will restrict the study to homogeneous flows for sake of clarity and simplification so that the diffusion terms vanishes and the variable $\boldsymbol{X}$ is omitted. Exiled in one-dimensional spectral space, the turbulence quantities become only functions of the scalar wave number rather than the full wave vector. The PITM equations are formally obtained from integration of equation (Eq. (5)) in the wave number ranges $[0,\kappa_c]$, $[\kappa_c,\kappa_d]$ and $[\kappa_d,\infty[$, where κ_c is the cutoff wave number linked to the filter size Δ by $\kappa_c = \pi/\Delta$, and κ_d is the dissipative wave number located at the far end of the inertial range of the spectrum assuming that the energy pertaining to higher wave numbers is negligible [10, 11]. As a result, one then obtain for each spectral region

$$\frac{\partial \tau_{ij\,[0,\kappa_c]}}{\partial t} = P_{ij\,[0,\kappa_c]} - \mathcal{F}_{ij}(\kappa_c,t) - \mathcal{K}_{ij}(\kappa_c,t) + \Pi_{ij\,[0,\kappa_c]} \quad (9)$$

$$\frac{\partial \tau_{ij\,[\kappa_c,\kappa_d]}}{\partial t} = P_{ij\,[\kappa_c,\kappa_d]} - \mathcal{F}_{ij}(\kappa_d,t) - \mathcal{K}_{ij}(\kappa_d,t) + \mathcal{F}_{ij}(\kappa_c,t) + \mathcal{K}_{ij}(\kappa_c,t) + \Pi_{ij\,[\kappa_c,\kappa_d]} \quad (10)$$

$$0 = F_{ij}(\kappa_d,t) - \epsilon_{ij\,[\kappa_d,\infty[} \quad (11)$$

where

$$\tau_{ij\,[0,\kappa_c]} = \int_0^{\kappa_c} \varphi_{ij}(\kappa,t)d\kappa \quad (12)$$

for the large resolved scales and

$$\tau_{ij\,[\kappa_c,\kappa_d]} = \int_{\kappa_c}^{\kappa_d} \varphi_{ij}(\kappa,t)d\kappa \quad (13)$$

for the smaller modeled scales. The redistribution term $\Pi_{ij\,[\kappa_c,\kappa_d]}$ is given by

$$\Pi_{ij\,[\kappa_c,\kappa_d]} = \int_{\kappa_c}^{\kappa_d} \Psi_{ij}(\kappa,t)d\kappa \quad (14)$$

The subgrid viscous dissipation-rate reads

$$(\epsilon_{ij})_{[\kappa_d,\infty[} = \int_{\kappa_d}^{\infty} \mathcal{E}_{ij}(\kappa,t)d\kappa \quad (15)$$

The total flux of energy transfer through the cutoff κ_c, is obtained from

$$F_{ij}(\kappa_c,t) = \mathcal{F}_{ij}(\kappa_c,t) + \mathcal{K}_{ij}(\kappa_c,t) \quad (16)$$

where

$$\mathcal{K}_{ij}(\kappa_c,t) = -\varphi_{ij}(\kappa_c,t)\frac{\partial \kappa_c}{\partial t} \quad (17)$$

with the definition

$$\mathcal{F}_{ij}(\kappa,t) = \int_{\kappa}^{\infty} \mathcal{T}_{ij}(\kappa',t)d\kappa' = -\int_0^{\kappa} \mathcal{T}_{ij}(\kappa',t)d\kappa' \quad (18)$$

Eq. (11) indicates that the tensorial dissipation-rate can be considered as a spectral flux that is independent of the cutoff wave number κ_c. Its theoretical expression is given by Eq. (15). Combining Eq. (10) with Eq. (11) results in the transport equation for the subgrid scale stress $\tau_{ij\,[\kappa_c,\kappa_d]}$ in the statistical sense

$$\frac{\partial \tau_{ij\,[\kappa_c,\kappa_d]}}{\partial t} = P_{ij\,[\kappa_c,\kappa_d]} + \mathcal{F}_{ij}(\kappa_c,t) - \varphi_{ij}(\kappa_c,t)\frac{\partial \kappa_c}{\partial t} + \Pi_{ij\,[\kappa_c,\kappa_d]} - (\epsilon_{ij})_{[\kappa_d,\infty[} \quad (19)$$

This equation allows to single out the role played by the term accounting for the variation of the cutoff wave number $\mathcal{K}_{ij}(\kappa_c,t)$ on the modeled/resolved scales. The corresponding transfer $\mathcal{K}(\kappa_c,t)$ associated with the turbulent kinetic energy can be also written [17, 18]

$$\mathcal{K}(\kappa_c,t) = -E(\kappa_c,t)\frac{\partial \kappa_c}{\partial t} = \frac{\partial k_{[\kappa_c,\kappa_d]}}{\partial \Delta}\frac{\partial \Delta}{\partial t} \quad (20)$$

showing clearly that it is a function of the derivative of the subgrid energy to the grid-size. In case the grid-size increases in time $\partial\Delta(t)/\partial t > 0$ or $\mathcal{K}(\kappa_c) > 0$, then a part of the energy contained into the resolved scales is removed and fed into the modeled spectral zone, whereas on the contrary, when $\partial\Delta(t)/\partial t < 0$ or $\mathcal{K}(\kappa_c) < 0$, a part of energy coming from the modeled zone is injected into the resolved scales [17, 18]. It is simple matter to show that $\tau_{ij\,[\kappa_c,\kappa_d]}$ corresponds in fact to the statistical averaging of the subgrid scale fluctuating velocities, more precisely

$$\tau_{ij\,[\kappa_c,\kappa_d]} = \langle (\tau_{ij})_{sfs}\rangle = \left\langle u_i^{>} u_j^{>}\right\rangle \quad (21)$$

where $(\tau_{ij})_{sfs}$ and $k_{sfs} = (\tau_{mm})_{sfs}/2$ denote the subfilter stress and subfilter energy, respectively, in the more general case where the filter is greater than the grid-size (as it has to be). Eq. (19) involving the evolution of

the subfilter-scale stress $(\tau_{ij})_{sfs}$ can be rewritten in an instantaneous form as

$$\frac{\partial(\tau_{ij})_{sfs}}{\partial t} = (P_{ij})_{sfs} + \frac{\partial(\tau_{ij})_{sfs}}{\partial\Delta}\frac{\partial\Delta}{\partial t} + (\Pi_{ij})_{sfs} - (\epsilon_{ij})_{sfs} \tag{22}$$

where

$$(P_{ij})_{sfs} = (P_{ij})_{[\kappa_c,\kappa_d]} + F_{ij}(\kappa_c) \tag{23}$$

$$(\Pi_{ij})_{sfs} = (\Pi_{ij})_{[\kappa_c,\kappa_d]} \tag{24}$$

$$(\epsilon_{ij})_{sfs} = (\epsilon_{ij})_{[\kappa_d,\infty[} \tag{25}$$

and in a contracted tensor form

$$\frac{\partial k_{sfs}}{\partial t} = P_{sfs} + \frac{\partial k_{sfs}}{\partial\Delta}\frac{\partial\Delta}{\partial t} - \epsilon_{sfs} \tag{26}$$

So, at the wavenumber κ_d, all the preceding hypotheses imply $F(\kappa_d) = \epsilon \approx \epsilon_{sfs}$, the turbulence Reynolds number being supposed to be large. Like in the RANS multiscale approach [21], the wavenumber κ_d is defined such that

$$\kappa_d - \kappa_c = \zeta\frac{\epsilon_{sfs}}{k_{sfs}^{3/2}} \tag{27}$$

where the value of the numerical coefficient ζ is chosen to ensure that the wavenumber κ_d is always sufficiently large in order to leave the entire inertial region. The dissipation rate equation is then obtained by taking the derivative of Eq. (27) with respect to time. Hence, one can easily obtain [9, 10, 14]

$$\frac{\partial\epsilon_{sfs}}{\partial t} = c_{\epsilon_1}\frac{\epsilon_{sfs}}{k_{sfs}}\Big(P_{sfs} + \frac{\partial k_{sfs}}{\partial\Delta}\frac{\partial\Delta}{\partial t}\Big) - c_{\epsilon_{2sfs}}\frac{\epsilon_{sfs}^2}{k_{sfs}} \tag{28}$$

with $c_{\epsilon_1} = \frac{3}{2}$. Then, it is also found [9, 10, 14] that

$$c_{\epsilon_{2sfs}} = \frac{3}{2} - \frac{k_{sfs}}{(\kappa_d - \kappa_c)\,E(\kappa_d)}\left[\left(\frac{\mathcal{F}(\kappa_d) - F(\kappa_d)}{\epsilon}\right) - \frac{E(\kappa_d)}{E(\kappa_c)}\left(\frac{\mathcal{F}(\kappa_c) - F(\kappa_c)}{\epsilon}\right)\right] \tag{29}$$

Setting $\kappa_d \gg \kappa_c$, and $E(\kappa_d) \ll E(\kappa_c)$, Eq. (29) reduces to

$$c_{\epsilon_{2sfs}}(\kappa_c) = \frac{3}{2} - \frac{k_{sfs}(\kappa_c)}{\kappa_d E(\kappa_d)}\left(\frac{\mathcal{F}(\kappa_d) - F(\kappa_d)}{\epsilon}\right) \tag{30}$$

which is valid for any value of κ_c. Considering this equation for $\kappa_c = 0$ so that $k_{sfs}(0) = k$ in pure RANS modelling, and combining Eq. (30) with this equation for $\kappa_c = 0$, it is then simple matter to show that [9, 10]

$$c_{\epsilon_{2sfs}} = \frac{3}{2} + \frac{k_{sfs}}{k}\left(c_{\epsilon_2} - \frac{3}{2}\right) \tag{31}$$

The numerical value $c_{\epsilon_1} = 3/2$ can be re-adjusted if necessary to a different value and the more general expression for $c_{\epsilon_{2sfs}}$ is [11]

$$c_{\epsilon_{2sfs}} = c_{\epsilon_1} + \frac{k_{sfs}}{k}\left(c_{\epsilon_2} - c_{\epsilon_1}\right) \tag{32}$$

The ratio k_{sfs}/k appearing in Eq. (31) can be calibrated as a function of the location of the cutoff wave number. In the first version of the PITM method [9, 10], this ratio was computed by integrating the Kolmogorov law in the wave number range $[\kappa_c, \infty[$ taking into account the limiting condition when k_{sfs} approaches k leading to

$$c_{\epsilon_{2sfs}} = c_{\epsilon_1} + \frac{c_{\epsilon_2} - c_{\epsilon_1}}{1 + \beta\eta_c^{2/3}} \tag{33}$$

where $\eta_c = \kappa_c L_e$, $L_e = k^{3/2}/\epsilon$ and $\beta = 2/(3C_K)$. Then, in more advanced PITM models, the universal spectrum [6]

$$E(\kappa) = \frac{\frac{2}{3}\beta(\kappa L_e)^{\alpha-1}L_e k}{[1 + \beta(\kappa L_e)^{\alpha}]^{\gamma+1}} \tag{34}$$

where α and β are constant coefficients given by $\alpha\gamma = 2/3$ and $\beta = [2/(3C_K)]^{\gamma}$ to comply with the Kolmogorov law, was considered to better describe the spectrum at the origin of small wave numbers. As known, in this region, the spectrum behaves like $E(\kappa) = \propto \kappa^{\alpha-1}$ taking into account the hypothesis of permanence of very large eddies. Using Eq. (34), it is a simple matter to compute the ratio k_{sfs}/k, leading to the more accurate computation of the coefficient $c_{\epsilon_{2sfs}}$ than Eq. (33) as

$$c_{\epsilon_{2sfs}} = c_{\epsilon_1} + \frac{c_{\epsilon_2} - c_{\epsilon_1}}{[1 + \beta\eta_c^{\alpha}]^{\gamma}} \tag{35}$$

In practice [5, 6, 19, 20, 22], the coefficients used in Eq. (34) are $\alpha = 3$ and $\gamma = 2/9$. This feature first introduced in [9, 10] was more recently imported into the PANS model [33] allowing decisive improvements. Unlike RANS closures, Eq. (35) sensitizes the model to the filter width [18, 17] (or in practice the grid-size Δ), and tends to draw the spectral distribution towards the prescribed equilibrium distribution given by Eq. (34). The set of the final transport equations for $(\tau_{ij})_{sfs}$ and ϵ_{sfs} accounting for non-homogeneous flows with varying filter width in time and space are given in Refs. [17, 18]. The different contributions appearing in Eq. (22) including the diffusion term read

$$(P_{ij})_{sfs} = -(\tau_{ik})_{sfs}\frac{\partial\bar{u}_j}{\partial x_k} - (\tau_{jk})_{sfs}\frac{\partial\bar{u}_i}{\partial x_k} \tag{36}$$

the redistribution term $(\Pi_{ij})_{sfs}$ is decomposed into a slow part $(\Pi_{ij}^1)_{sfs}$ that characterizes the return to isotropy due to the action of subgrid turbulence on itself

$$(\Pi_{ij}^1)_{sfs} = -c_1\frac{\epsilon_{sfs}}{k_{sfs}}\left((\tau_{ij})_{sfs} - \frac{1}{3}(\tau_{mm})_{sfs}\delta_{ij}\right) \tag{37}$$

and a rapid part, $(\Pi_{ij}^2)_{sfs}$ that describes the action of the filtered velocity gradients

$$(\Pi_{ij}^2)_{sfs} = -c_2\left((P_{ij})_{sfs} - \frac{1}{3}(P_{mm})_{sfs}\,\delta_{ij}\right) \tag{38}$$

where c_1 plays the same role as the Rotta coefficient but is no longer constant whereas c_2 is the same coefficient used in RANS modelling. The diffusion terms $(J_{ij})_{sfs}$ is modeled assuming a well-known gradient law

$$(J_{ij})_{sfs} = \frac{\partial}{\partial x_m}\left(\nu\frac{\partial(\tau_{ij})_{sfs}}{\partial x_m} + c_s\frac{k_{sfs}}{\epsilon_{sfs}}(\tau_{ml})_{sfs}\frac{\partial(\tau_{ij})_{sfs}}{\partial x_l}\right) \tag{39}$$

where c_s is a constant coefficient. The diffusion term $(J_\epsilon)_{sfs}$ included in Eq. (28) reads

$$(J_\epsilon)_{sfs} = \frac{\partial}{\partial x_j}\left(\nu\frac{\partial\epsilon_{sfs}}{\partial x_j} + c_\epsilon\frac{k_{sfs}}{\epsilon_{sfs}}(\tau_{jm})_{sfs}\frac{\partial\epsilon_{sfs}}{\partial x_m}\right) \tag{40}$$

where c_ϵ is a constant coefficient. In a general way, the derivative $\partial\bar{\phi}/\partial\Delta$ can be computed is computed by applying a second filtering operation with a larger filter width leading to

$$\frac{\partial\bar{\phi}}{\partial\Delta} = \lim_{\delta\Delta\to 0}\frac{\bar{\phi}(\bar{\Delta}+\delta\bar{\Delta})-\bar{\phi}(\bar{\Delta})}{\delta\bar{\Delta}} \approx \frac{\bar{\phi}(\widetilde{\bar{\Delta}})-\bar{\phi}(\bar{\Delta})}{\widetilde{\bar{\Delta}}-\bar{\Delta}} \quad (41)$$

where $\bar{\Delta}$ is the filter width of the grid-size Δ, and $\widetilde{\bar{\Delta}}$ denotes the superfilter width of Δ. Eq. (41) can be applied easily for the the subfilter scale stress $(\tau_{ij})_{sfs}$ with respect to the filter width $\bar{\Delta}$ leading to [17]

$$\frac{\partial(\tau_{ij})_{sfs}}{\partial\Delta} \approx \frac{(\tau_{ij})_{sfs}(\widetilde{\bar{\Delta}})-(\tau_{ij})_{sfs}(\bar{\Delta})}{\widetilde{\bar{\Delta}}-\bar{\Delta}} = \frac{(\widetilde{\overline{u_iu_j}}-\widetilde{\bar{u}}_i\widetilde{\bar{u}}_j)-(\overline{u_iu_j}-\bar{u}_i\bar{u}_j)}{\widetilde{\bar{\Delta}}-\bar{\Delta}} \quad (42)$$

The transfer flux $\mathcal{K}(\kappa_c)$ can be computed from tensorial contraction of Eq. (42) but also in a theoretical way from Eq. (34) as in [17]

$$\mathcal{K}(\kappa_c) = \frac{2}{3}\beta(\pi L_e)^\alpha\left(\frac{k_{sfs}}{k}\right)^{\frac{\gamma+1}{\gamma}}\frac{k}{\Delta^{\alpha+1}}\frac{\partial\Delta}{\partial t} \quad (43)$$

Note that these commutation terms like in Eq. (26) are needed explicitly only for strong variations in mesh density.

2.2.2 Turbulent passive scalar field

It is possible to extend the PITM method developed for dynamic turbulent fields to scalar fields. In the following, we will only indicates the basic guidelines leading to the variance and scalar dissipation equations of a passive scalar. The key is to work in the spectral space. The spectral transport equation of the scalar variance denoted $E_\theta(\boldsymbol{X},\kappa) = \langle\theta'\theta'(\boldsymbol{X})\rangle^\Delta(\kappa)/2$ reads [23]

$$\frac{\partial E_\theta(\boldsymbol{X},\kappa)}{\partial t} + \langle u_k\rangle(\boldsymbol{X})\frac{\partial E_\theta(\boldsymbol{X},\kappa)}{\partial X_k} = \mathcal{P}_\theta(\boldsymbol{X},\kappa) + \mathcal{T}_\theta(\boldsymbol{X},\kappa) + \mathcal{J}_\theta(\boldsymbol{X},\kappa) - \mathcal{E}_\theta(\boldsymbol{X},\kappa) \quad (44)$$

where in the right hand side of this equation, $\mathcal{P}_\theta$ is the production of half the scalar variance by mean gradients of the scalar, $\mathcal{T}_\theta$ is the spectral transfer driven by the eddying motions in the inertial cascade, $\mathcal{J}_\theta$ is the diffusion term and $\mathcal{E}_\theta$ denotes the dissipation term of half the scalar variance. In particular, the production term $\mathcal{P}_\theta$ is defined by

$$\mathcal{P}_\theta(\boldsymbol{X},\kappa) = -\varphi_{j\theta}(\boldsymbol{X},\kappa)\frac{\partial\langle\theta\rangle}{\partial X_j} \quad (45)$$

where $\varphi_{j\theta}(\boldsymbol{X},\kappa,t) = \left\langle u_j'\theta'(\boldsymbol{X})\right\rangle^\Delta(\kappa,t)$ whereas the dissipation term reads

$$\mathcal{E}_\theta(\boldsymbol{X},\kappa) = \frac{\sigma}{2}\frac{\partial^2 E_\theta(\boldsymbol{X},\kappa)}{\partial X_j\partial X_j} + 2\sigma\kappa^2 E_\theta(\boldsymbol{X},\kappa) \quad (46)$$

where σ denotes the molecular diffusivity computed as $\sigma = \nu/Pr$ using the molecular Prandtl number Pr. Eq. (44) can be integrated in the same way as Eq. (5) but in the domains $[0,\kappa_c]$, $[\kappa_c,\kappa_e]$ and $[\kappa_e,\infty[$ where κ_e denotes here the high end wave number that can be larger or smaller than κ_c and different from κ_d, leading to the resulting equations

$$\frac{\partial k_{\theta[0,\kappa_c]}}{\partial t} = P_{\theta[0,\kappa_c]} - \mathcal{F}_\theta(\kappa_c,t) - \mathcal{K}_\theta(\kappa_c,t) \quad (47)$$

$$\frac{\partial k_{\theta[\kappa_c,\kappa_e]}}{\partial t} = P_{\theta[\kappa_c,\kappa_e]} - \mathcal{F}_\theta(\kappa_e,t) - \mathcal{K}_\theta(\kappa_e,t) + \mathcal{F}_\theta(\kappa_c,t) + \mathcal{K}_\theta(\kappa_c,t) \quad (48)$$

$$0 = F_\theta(\kappa_e) - \epsilon_{\theta[\kappa_e,\infty[} \quad (49)$$

where

$$k_{\theta[0,\kappa_c]} = \int_0^{\kappa_c} E_\theta(\kappa,t)d\kappa \quad (50)$$

$$k_{\theta[\kappa_c,\kappa_e]} = \int_{\kappa_c}^{\kappa_e} E_\theta(\kappa,t)d\kappa \quad (51)$$

$$(\epsilon_\theta)_{[\kappa_e,\infty[} = \int_{\kappa_e}^{\infty}\mathcal{E}_\theta(\kappa,t)d\kappa \quad (52)$$

The total flux of variance $F_\theta(\kappa)$ at the wave number κ_c of the spectrum E_θ is then given by

$$F_\theta(\kappa_c,t) = \mathcal{F}_\theta(\kappa_c,t) + \mathcal{K}_\theta(\kappa_c,t) \quad (53)$$

where

$$\mathcal{K}_\theta(\kappa_c,t) = -E_\theta(\kappa_c,t)\frac{\partial\kappa_c}{\partial t} \quad (54)$$

with the definition

$$\mathcal{F}_\theta(\kappa,t) = \int_\kappa^\infty\mathcal{T}_\theta(\kappa',t)d\kappa' = -\int_0^\kappa\mathcal{T}_\theta(\kappa',t)d\kappa' \quad (55)$$

The subfilterscale variance of the passive scalar is defined as $k_{\theta[\kappa_c,\kappa_e]} = \left\langle k_{\theta sfs}\right\rangle = \left\langle\theta^>\theta^>\right\rangle/2$. Combining these equations, it is simple matter to show that Eq. (48) can be rewritten as in an instantaneous form as

$$\frac{\partial k_{\theta sfs}}{\partial t} = P_{\theta[\kappa_c,\kappa_e]} + F_\theta(\kappa_c,t) - \epsilon_\theta \quad (56)$$

where Eq. (56) expresses simply that the subfilter turbulence scalar variance is computed as the integral of the variance density in the interval $[\kappa_c,\kappa_e]$, considering that the variance in the zone $[\kappa_e,\infty[$ is negligible. As the flux transfer at κ_e approaches the dissipation $F_\theta(\kappa_e) \approx \epsilon_\theta$, like in Eq. (27), the wave numbers κ_e and κ_c can be then related in a such way that $\kappa_e - \kappa_c = \mathcal{O}(1/l_\theta) = \mathcal{O}(\epsilon_\theta/\theta^2 u)$. Following the same mathematical framework as in the preceding section step by step, considering moreover the counterpart of Eq. (27) transposed to the case of scalar fields, one can derive easily the transport equation of ϵ_θ as for [25]

$$\frac{\partial\epsilon_\theta}{\partial t} = c_{\epsilon_{\theta\theta_1}}P_{\theta sfs}\frac{\epsilon_\theta}{k_{\theta sfs}} + c_{\epsilon_{\theta k_1}}P_{sfs}\frac{\epsilon_\theta}{k_{sfs}} - c_{\epsilon_{\theta k_2}}\frac{\epsilon_\theta\epsilon}{k_{sfs}} - c_{\epsilon_{\theta\theta_{2sfs}}}\frac{\epsilon_\theta^2}{k_{\theta sfs}} \quad (57)$$

with

$$P_{\theta sfs} = P_{\theta[\kappa_c,\kappa_e]} + F_\theta(\kappa_c) \quad (58)$$

and where $c_{\epsilon_{\theta\theta_1}}$, $c_{\epsilon_{\theta k_1}}$, $c_{\epsilon_{\theta k_2}}$ are constant coefficients whereas $c_{\epsilon_{\theta\theta_{2sfs}}}$ is now a dynamical coefficient involving both the wave numbers κ_c and κ_e. For non-homogeneous flows, the diffusion terms J_θ and J_{ϵ_θ} modeled assuming the well-known tensorial gradient law hypothesis are included into Eq. (56) and Eq. (57). At least, note that Eq. (22), Eq. (26), Eq. (28), Eq. (56), Eq. (57) to be solved in the PITM method require appropriate numerical schemes both in time and space that are more accurate than schemes used in the traditional RANS method [26].

2.3 Illustrations to several typical turbulent flows

2.3.1 An overview

Several turbulent flows of complex physics have been performed using the PITM method to this day. Among these flows, it is worth mentioning pulsed flows [9], the mixing of turbulent flow fields of differing scales [27], thermal convection at high Rayleigh numbers [31], rotating flows encountered in turbomachinery at the bulk Reynolds number $R_b = U_b\delta/\nu = 14000$ and at different rotation numbers $R_o = \Omega\delta/U_b$ varying from moderate, medium and very high rotation rates $R_o = 0.17$, 0.50 and 1.50 [20], flows with appreciable fluid injection through the surface which correspond to the propellant burning in solid rocket motors [10], flows over periodic hills with separation and reattachment of the boundary layer both at the Reynolds number $Re = 10595$ [24, 28, 29] and $Re = 37000$ [5], flow subjected to axisymmetric contraction [22], airfoil flows at the Reynolds number $Re = 1.64 \times 10^6$ for an angle of attack 12° [30]. In the following, we point out and discuss some results obtained for the flow over periodic hills involving turbulence mechanisms associated with separation, recirculation, reattachment, acceleration and wall effects.

2.3.2 The turbulent flow over periodic hills at high Reynolds number

This flow was investigated experimentally at the two Reynolds numbers $Re = U_b h/\nu$ =10595 and 37000 based on the hill height h and the bulk velocity U_b about the hill crest [32] and performed by Chaouat [24], Chaouat and Schiestel [5]. Overall, it is found that the PITM re-

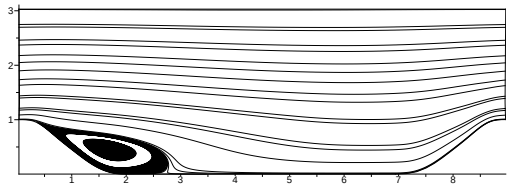

(a)

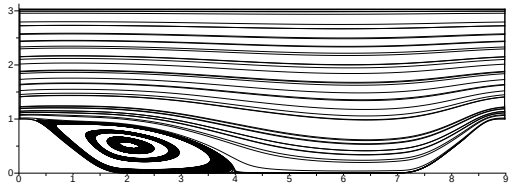

(b)

Figure 1: Streamlines of the average flowfield at Re=10595. (a) RSM computation ($80 \times 30 \times 100$); (b) PITM simulation ($160 \times 60 \times 100$).

produced fairly well this flow according to reference data [32] while the RSM computation returned some weakness in the predictions. Figures 1 and 2 show the streamlines plot for the RSM computation and PITM simulation, respectively. For the PITM, the plot are generated in two dimensions and obtained by averaging the velocities both in the homogeneous planes in the spanwise direction and in time. The flow separation that is clearly visible is caused by the adverse pressure gradient resulting from

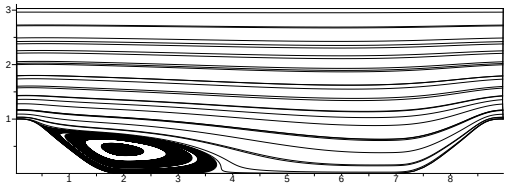

(a)

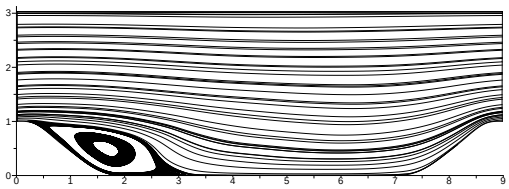

(b)

Figure 2: Streamlines of the average flowfield at Re=37000. (a) RSM computation ($80 \times 30 \times 100$); (b) PITM simulation ($160 \times 60 \times 100$).

the strong streamwise curvature of the lower wall. Due to the flow recirculation, a strong turbulence activity is visible near the lower wall and this one is particularly concentrated in the leeward region of the second hill. At $Re = 10595$, the RSM model predicted a too small recirculation zone probably because the model cannot capture the large eddies naturally issued from the streamwise curvature of the lower wall that play a major role in this type of flow. At $Re = 37000$, the recirculation zone was on the contrary strongly under-predicted in comparison with those measured from the experiment, mainly because the separation is delayed. These flows were investigated in details in Refs [24, 5] showing the mean velocity and turbulent stress profiles in several sections of the channel with a comprehensive study.

3 Conclusions

The PITM method allowing seamless coupling between RANS and LES regions has been developed to perform numerical simulations of turbulent flows out of spectral equilibrium on relatively coarse grids to overcome the practical difficulties posed by LES. Unlike almost hybrid RANS/LES models that are built upon empirical techniques, the PITM method relies on a mathematical framework developed in spectral space that provides valuable physical grounds. We hope that this contribution will open promising routes for new future heuristic developments in hybrid RANS/LES modelling.

References

[1] R. Schiestel, *Modeling and simulation of turbulent flows*, ISTE Ltd and J. Wiley, 2008.

[2] K. Hanjalic, B.E. Launder, *Modelling turbulence in engineering and the environment. Second-moment route to closure*, Cambridge University Press, 2011.

[3] M. Leschziner, M.N. Li and F. Tessicini, Simulating flow separation from continuous surfaces: routes

to overcoming the Reynolds number barrier, Phil. Trans. R. Soc. A **367**, 2885-2903, 2009.

[4] B. Chaouat, Reynolds stress transport modeling for high-lift airfoil flows, AIAA Journal, **44**, 2390-2403, 2006.

[5] B. Chaouat and R. Schiestel, Hybrid RANS-LES simulations of the turbulent flow over periodic hills at high Reynolds number using the PITM method, Computers and Fluids **84**, 279-300, 2013.

[6] B. Chaouat, The state of the art of hybrid RANS/LES modeling for the simulation of turbulent flows, Flow, Turbulence and Combustion, **99**(2), 279-327, 2017.

[7] C.G. Speziale, Turbulence modeling for time-dependent RANS and VLES: A review, AIAA Journal, **36**, 173-184, 1998.

[8] P.R. Spalart, Detached-eddy simulation, Annual. Review Fluid Mechanics, **41**, 181-202, 2009.

[9] R. Schiestel and A. Dejoan, Towards a new partially integrated transport model for coarse grid and unsteady turbulent flow simulations, Theoretical and Computational Fluid Dynamics, **18**, 443-468, 2005.

[10] B. Chaouat and R. Schiestel, A new partially integrated transport model for subgrid-scale stresses and dissipation rate for turbulent developing flows, Physics of Fluids, **17**, 065106, 1-19, 2005.

[11] B. Chaouat and R. Schiestel, Analytical insights into the partially integrated transport modeling method for hybrid Reynolds averaged Navier-Stokes equations-large eddy simulations of turbulent flows, Physics of Fluids, **24**, 085106, 1-34, 2012.

[12] S.S. Girimaji, Partially-averaged Navier-Stokes method for turbulence: A Reynolds -averaged Navier-Stokes to direct numerical simulation bridging method, Journal of Applied Mechanics, ASME, **73**, 413-421, 2006.

[13] F.R. Menter and Y. Egorov, The scale-adaptive simulation method for unsteady turbulent flow prediction: Part 1: Theory and model description, Flow, Turbulence and Combustion, **85**, 113-138, 2010.

[14] B. Chaouat and R. Schiestel, From single-scale turbulence models to multiple-scale and subgrid-scale models by Fourier transform, Theoretical and Computational Fluid Dynamics, **21**, 201-229, 2007.

[15] B. Chaouat and R. Schiestel, Simulations of turbulent flows out of a spectral equilibrium using the PITM method, *23ème Congrès Français de Mécanique*, 2491-715X, 1-16, 2017.

[16] C. Cambon, D. Jeandel and J. Mathieu, Spectral modelling of homogeneous non-isotropic turbulence, Journal of Fluid Mechanics, **104**, 247-262, 1981.

[17] B. Chaouat, Commutation errors in PITM simulations, International Journal of Heat and Fluid Flow, **67**, 138-154, 2017.

[18] B. Chaouat and R. Schiestel, Partially integrated transport modeling method for turbulence simulation with variable filters, Physics of Fluids, **25**, 125102, 1-39, 2013.

[19] B. Chaouat and R. Schiestel, Progress in subgrid-scale transport modelling for continuous hybrid non-zonal RANS/LES simulations, International Journal of Heat and Fluid Flow, **30**, 602-616, 2009.

[20] B. Chaouat, Simulation of turbulent rotating flows using a subfilter scale stress model derived from the partially integrated transport modeling method, Physics of Fluids, **24**, 045108, 1-35, 2012.

[21] R. Schiestel, Multiple-time scale modeling of turbulent flows in one point closures, Physics of Fluids, **30**, 722-731, 1987.

[22] B. Chaouat, Application of the PITM method using inlet synthetic turbulence generation for the simulation of the turbulent flow in a small axisymmetric contraction, Flow, Turbulence and Combustion, **98**(4), 987-1024, 2017.

[23] A. S. Monin and A. M. Yaglom *Statistical Fluid Mechanics*, The M.I.T. Press Cambridge, Massachusetts, vols. I and II, 1975.

[24] B. Chaouat, Subfilter-scale transport model for hybrid RANS/LES simulations applied to a complex bounded flow, Journal of Turbulence, **11**, 1-30, 2019.

[25] B. Chaouat and R. Schiestel, Passive scalar fluctuations in turbulent flows simulation in the framework of the partially integrated transport modeling method. *Submitted paper*, 2019.

[26] B. Chaouat, An efficient numerical method for RANS/LES turbulent simulations using subfilter scale stress transport equations, Int. J. Numer. Methods Fluids 67, 1207-1233, 2011.

[27] I. Befeno and R. Schiestel, Non-equilibrium mixing of turbulence scales using a continuous hybrid RANS/LES approach: Application to the shearless mixing layer, Flow, Turbulence and Combustion, **78**, 129-151, 2007.

[28] S. Jakirlic, S. Saric, G. Kadavelil, E. Sirbubalo, B. Basara and B. Chaouat, SGS modelling in LES of wall-bounded flow using transport RANS model: From a zonal to a seamless hybrid LES/RANS method, in *Proceedings of the 6th Symposium on Turbulence Shear Flow Phenomena*, edited by Seoul National University, vol. 3, 1057-1062, 2009.

[29] C. Friess, R. Manceau and T.B. Gatski, Toward an equivalence criterion for hybrid RANS/LES methods, Comput. Fluids **122**, 233-246, 2015.

[30] M. Stoellinger, R. Roy, and S. Heinz, Unified RANS-LES method based on second-order closure, in *Proceedings of the 9th Symposium on Turbulence Shear Flow Phenomena*, edited by The University of Melbourne, 7B5, 1-6, 2015.

[31] S. Kenjeres and K. Hanjalic, LES, T-RANS and hybrid simulations of thermal convection at high *Ra* numbers, Int. J. Heat Fluid Flow, **27**, 800-810, 2006.

[32] C. Rapp and M. Manhart, Flow over periodic hills - an experimental study, Experiments in Fluids, **51**, 247-269, 2011.

[33] H. Foroutan and S. Yavuzkurt, A partially-averaged Navier-Stokes model for the simulation of turbulent swirling flows with vortex breakdown, Int J Heat Fluid Flow, **50**, 402-416, 2014.